Organoselenium Compounds as Acetylcholinesterase Inhibitors: Evidence and Mechanism of Mixed Inhibition

Amit Kumawat, Shabnam Raheem, Fasil Ali, Tanveer Ali Dar, Suman Chakrabarty, and Masood Ahmad Rizvi

The Journal of Physical Chemistry B 2021, 125, 6, 1531–1541

Organoselenium Compounds as Acetylcholinesterase Inhibitors: Evidence and Mechanism of Mixed Inhibition

Amit Kumawat[1], Shabnam Raheem[2], Fasil Ali[3], Tanveer Ali Dar[3], Suman Chakrabarty*[,1] and Masood Ahmad Rizvi*[,2]

[1]Department of Chemical, Biological & Macromolecular Sciences, S. N. Bose National Centre for Basic Sciences, Kolkata 700106, India.

[2]Department of Chemistry, University of Kashmir, Srinagar, 190006, J&K, India.

[3]Department of Clinical Bio-Chemistry, University of Kashmir, Srinagar, 190006, J&K, India.

* Corresponding Authors

Email: sumanc@bose.res.in, masoodku2@gmail.com

Abstract

Acetylcholinesterase (AChE) inhibitors are actively used for the effective treatment of Alzheimer's disease. In recent years, the neuroprotective effects of organoselenium compounds such as Ebselen and Diselenides onto the AChE activity have been investigated as potential therapeutic agents. In this work we have carried out systematic kinetic and intrinsic fluorescence assays in combination with docking and molecular dynamics (MD) simulations to elucidate the molecular mechanism of the mixed inhibition of AChE by Ebselen and Diphenyl diselenide (DPDSe) molecules. Our MD simulations demonstrate significant heterogeneity in the binding modes and allosteric hotspots for DPDSe on AChE due to non-specific interactions. We have further identified that both Ebselen and DPDSe can strongly bind around the Peripheral Anionic Site (PAS) leading to non-competitive inhibition similar to other PAS binding inhibitors. We also illustrate the entry of DPDSe molecule into the gorge through a "side door", which offers an alternate entry point of AChE inhibitors as compared to the usual substrate entry point of the gorge. Together with results from experiments, these simulations provide mechanistic insights into the mixed type of inhibition for AChE using DPDSe as a promising inhibitor for AChE.

Introduction

Acetylcholinesterase (EC 3.1.1.7) (AChE), is a serine protease which plays a pivotal role in memory and cognition through its ability to hydrolyse the neurotransmitter acetylcholine to acetate and choline at cholinergic brain synapses[1]. Since its discovery, AChE has been extensively studied and has been the primary targets of insecticides and nerve agents[2]. Increasing evidences are found that correlate the activity of AChE to several neurodegenerative disorders like Alzheimer's disease (AD), Parkinson's disease (PD) etc[3,4]. Moreover, the impairment of cholinergic neuronal system in brain has been reported to be the underlying event of impairment of learning and memory in several animal models. Thus, inhibition of the AChE activity with the anticholinergic agents has therapeutic implications in countering diseases such as myasthenia gravis, glaucoma and AD[5-7].

Several experimental and theoretical studies have been devoted to investigate the mechanism of inhibition of AChE by the repertoire of AChE inhibitors (AChEIs)[8-12]. Previous structural studies have been shown to characterize the overall structure of the enzyme into several subsites: the active site (CAS) consisting of catalytic triad, anionic subsite (AS) and acyl binding pocket, and the peripheral anionic site (PAS) at the mouth of the gorge leading to active site[13,14]. Interestingly, the active site is buried at the bottom of this narrow gorge lined with conserved aromatic residues. The AChEIs have been found to either inhibit the enzyme through covalent modification of the active site or by allosteric regulation through significant conformational changes in the enzyme. Several computational studies together with X-ray crystallography have suggested existence of multiple access pathways to the active site that are implicated in substrate entry or product release (Fig. 1)[15-17]. In addition to the main entrance/exit along the gorge, alternative routes such as back door (involving residues W83, V129, Y446 etc based on mAChE residue numbering; PDB ID: 1C2B[18]) and side door (perpendicular to the gorge and comprising of residues from the omega loop) have been identified through molecular dynamics simulations and multiple copy sampling studies[19,20]. Cheng and coworkers have identified dynamic correlation between different subdomains in the protein and the

variation in the gorge radius[21]. Recently, several allosteric sites have been identified in AChE that can be helpful in the discovery of new allosteric inhibitors.

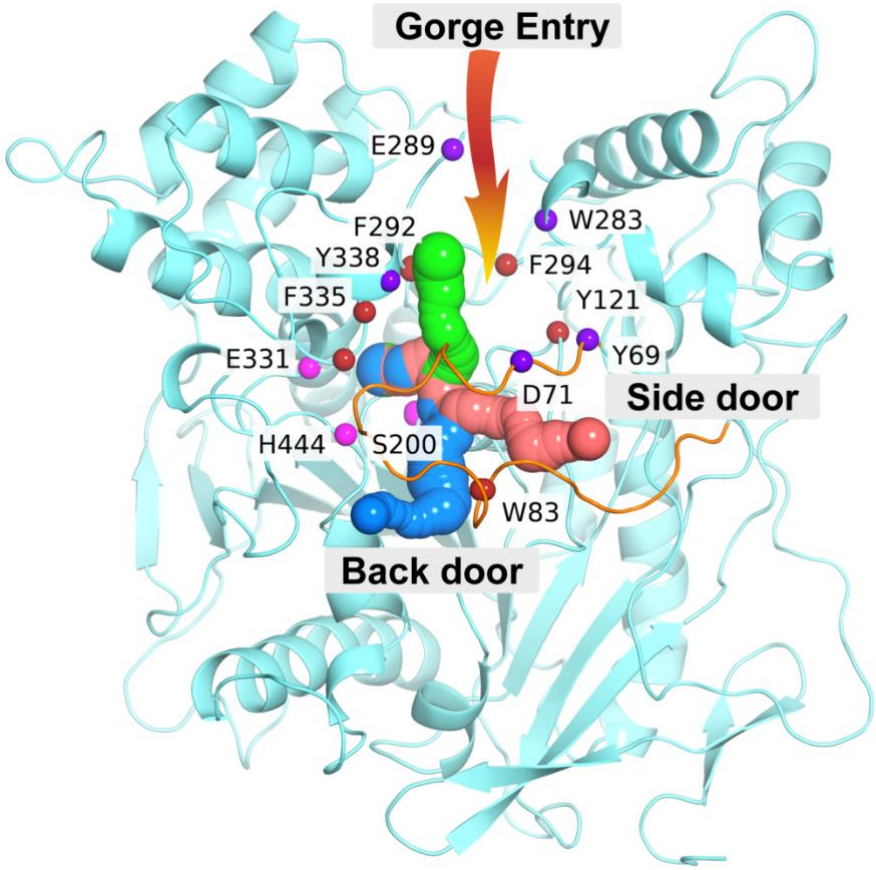

Figure 1. Representative image of crystal structure to highlight the structural features in AChE (PDB ID: 1C2B). The peripheral site residues, neck residues and catalytic residues are represented as spheres coloured in violet, red and magenta respectively. Previous studies highlight the existence of multiple routes of access to the active sites in AChE for the ligand molecules. These paths involve entry/exit through the mouth of the gorge (main pathway), back door that comprises residues W83, V129, Y446 and side door through the omega loop (orange colour). The cavities are represented as tunnels in green, blue and pink colours, respectively.

Currently approved U.S. FDA drugs such as tacrine, donepezil, rivastigmine and galantamine for the treatment of neurogenetic disorders (dementia, AD, traumatic brain injury and delirium) are primarily reversible competitive and non-competitive AChE inhibitors[22]. However, these drugs have poor bioavailability and are associated with a number of side effects, including gastrointestinal upsets, hepatotoxicity, increased risk of bradycardia and syncope (fainting). A great deal of research has been focused on the development of new therapeutics that includes derivatives, natural AChE inhibitors and hybrids with better efficacy and lesser side effect profile[23]. In this context, since more than last two decades, an increased interest has been generated in the study of organoselenides as anticancer lead compounds and their use in treatment of neurological disorders owning to the higher biodisposability rate and biological activity[24-26]. These compounds are known to show antioxidant properties, along with anti-inflammatory and neuroprotective role *in vitro* and *in vivo* experimental models[27]. Ebselen (Scheme 1) was first organoselenium compound with promising antioxidant and cognitive enhancer properties[28,29]. In fact, extensive work has been done in evaluation of pharmacological properties of ebselen to use it as a potential anti-AD agent[30]. In previous studies, several structural modifications to ebselen were made to synthesize novel molecules with enhanced antioxidative properties which include fusion of ebselen with previously known AChEIs (donepezil, tacrine)[31-33]. Diphenyl diselenide (DPDSe; Scheme 1) is another classical organoselenium compound that has proved to be a promising drug in a number of experimental studies of oxidative stress[34]. DPDSe has been shown to be even more active as a Glutathione Peroxidase (GPx) mimic and less toxic than ebselen[35]. More importantly, experimental and clinical studies have demonstrated a positive role of DPDSe in the cognitive performance with its involvement in the cholinergic system[34]. Previous data suggest that systemic administration or sub-chronic exposure to DPDSe ameliorates the impairment of spatial long-term and short-term recognition memory in mice and rat models. Recently, derivatives of DPDSe were studied to show inhibition of AChE activity in mice models exhibiting sporadic Alzeimer's-type dementia[36,37]. However, studies on the inhibitory effect of DPDSe on AChE are largely unexplored.

In continuation of our interests in exploring chemico-biological interactions of systems[24-26,38,39], the present study was therefore designed to elucidate the DPDSe induced inhibition of AChE and for identification of any novel allosteric binding sites. For this purpose, structural and functional integrity of AChE in the presence of DPDSe was evaluated through *in vitro* and *in silico* (molecular docking and simulation) approaches with ebselen as a control.

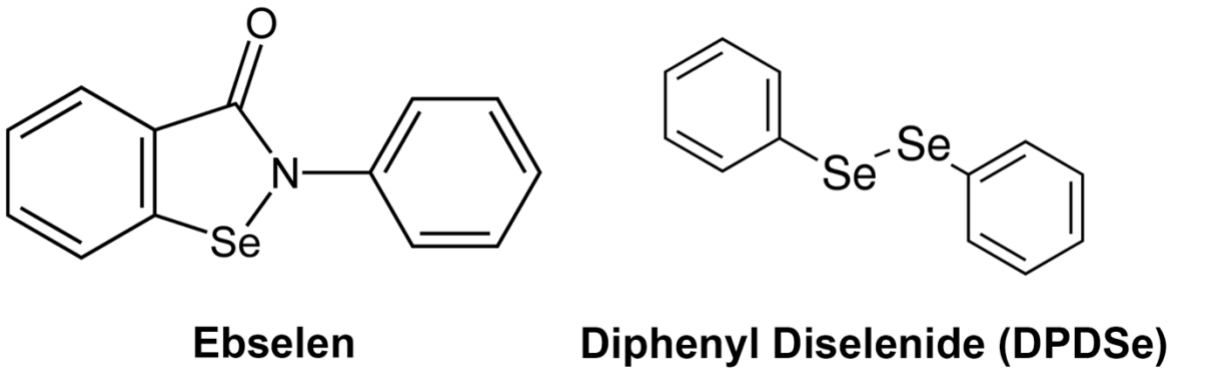

Scheme 1: Chemical structures of Ebselen and DPDSe

Materials and methods

Diphenyl diselenide (CAS number: 1666-13-3) and Ebselen (CAS number: 60940-34-3) were purchased from Sigma Aldrich and used as such without further purification.

Acetylcholinesterase inhibition assay

For measuring Acetylcholinesterase activity in presence of organoselenide inhibitors, modified method of Ellman *et al.* was used[40]. Acetylthiocholineiodide (ATCI) was used as substrate for measuring the AChE activity. Reaction mixture containing 150µL of AChE and increasing concentration of the inhibitors (1, 10, 50 and 100µM), was made upto 2.5mL by adding 50mM tris buffer of *p*H 7.0. After thorough mixing and preincubation of the reaction mixture for 6 hrs at 25^{o}C, the reaction was initiated by addition of 100µL of ATCI (15mM) which was followed by addition of 500µL of DTNB as colour indicator. Hydrolysis of ATCI to thiocholine by AChE was followed for 10 minutes by monitoring the formation of 5-thio-2-nitrobenzoate anion, as a coloured

product due to reaction between DTNB and thiocholine, Change in the absorbance was followed at 412nm using Cary-300 UV/Vis spectrophotometer, Agilent, USA.

Intrinsic Fluorescence

Intrinsic fluorescence measurement of AChE in the absence and presence of varying ebselen and DPDSe concentrations (0.0, 1.0, 10, 50 and 100µM) were recorded in triplicates over a wavelength range of 300-500 nm using Agilent Cary Eclipse fluorescence spectrophotometer. Upon excitation of AChE at a wavelength of 280nm, tryptophan residues of AChE showed maximum emission at 334nm. During the entire run, scanning speed was kept as 5nm/min with excitation and emission filter width of 5nm.

Molecular modelling and docking

The Glide XP (Schrodinger Suite, Version 2019.4) protocol[41] was used to perform the molecular docking analysis of the compounds, ebselen and DPDSe into the catalytic site of AChE. The crystal structure used for docking was in the ligand-unbound monomer form (*apo* form, PBD ID: 1C2B)[18]. The receptor grid was defined based on the key gorge residues identified in previous studies. While the receptor was kept rigid all possible conformers of the ligands were generated by the LigPrep utility of Schrodinger Suite. The binding poses with best docking scores for Ebselen and DPDse were selected for further MD simulations and binding energy calculations.

Molecular dynamics (MD) simulations

MD simulations were performed using crystal structure of acetylcholinesterase (AChE) (PDB ID: 1C2B)[18]. The starting structure of AChE for all the simulations was in the *apo* monomer form (ligand unbound). The missing residues/side-chains were incorporated using using Modeller. The protonation states of the titrable residues were assigned based on the pKa estimated by PROPKA-3.0. One set of MD simulations were performed using the docked complexes for ebselen and DPDSe bound states of AChE. Another set of ligand exploratory simulations were performed where the *apo* form was placed at the centre of the box and all binding simulations with the ligand were initiated by placing the

ligand molecules at random positions in the solvent-filled simulation box. The ligand was allowed to diffuse freely and no bias was added for the space exploration.

All simulations were performed using GROMACS 5.1.4 software[42] using two different set of force fields to test the consistency of the observations irrespective of the choice of force field. In one set of simulations for the AChE-DPDSe system, AmberSB99-Ildn forcefield[43] and the TIP4P-Ew water model[44] was used. In another set GROMOS54a7 forcefield[45] and SPC water model[46] were used to simulate both the AChE-DPDSe and AChE-Ebselen systems. General AMBER force field (GAFF)[47] parameters for DPDSe were generated using the Antechamber utility of AmberTools18. Since certain parameters for Ebselen could not be generated using GAFF, we have adopted GROMOS force field using ATB web server[48] to compare both Ebselen and DPDSe in the same footing. The systems were inserted into cubic box with a margin of at least 1.2nm in each direction resulting in a ~10.5nm wide box for all simulations. The solvated systems were neutralized by adding counter ions and appropriate number of Na^+ and Cl^- ions were added to maintain salt concentration of 150mM.

All systems were energy minimized using steepest descent method followed by two step equilibration in NVT and NPT ensembles. The temperature was maintained at 300K using velocity rescale method[49] with a relaxation time of 1ps and pressure was kept constant at 1atm using Parinello-Rahman barostat[50]. All simulations were performed using periodic boundary conditions and the long range interactions were calculated using particle mesh Ewald (PME) summation method[51]. The cut-off distance for electrostatic and van der Waals interactions was set to 1.0nm. The bonds were constrained with LINCS[52] and the integration time step was set to 2fs. The atomistic MD simulation for the apo form was performed for 400ns. MD simulation runs were performed for the docked structures with ebselen and DPDSe for 200ns. In addition, we have generated 4 independent trajectories (500ns-1μs long) each for Ebselen and DPDSe freely inserted into the simulation box in order to explore alternative binding sites other than the gorge (identified by docking).

Binding energy calculations (MM/PBSA)

The binding energies for the compounds, Ebselen and DPDSe with AChE were calculated using the MM/PBSA method[53]. The g_mmpbsa utility developed by Kumari *et. al*. combining the Gromacs package and APBS software was used to calculate the different energy contributions in the MM/PBSA binding energy including the electrostatic, polar and non-polar solvation energy terms[54]. We have calculated the binding energy of the ebselen and DPDSe molecules at the different binding sites by using snapshots at every 50ps from different segments of trajectory with respect to the ligand bound state.

Ideally the binding free energy of a protein-ligand complex should include both the entropic and enthalpic components, namely the interaction energy between ligand and protein (ΔE_{MM}, enthalpic part), the solvation energy associated with the transition of the ligand from bulk water to the binding site (ΔG_{Solv}), and the change in conformational entropy associated with ligand binding ($-T\Delta S$):

$$\Delta G_{bind} = \Delta E_{MM} + \Delta G_{solv} - T\Delta S \qquad (1)$$

Within the MM/PBSA framework, the binding energy is estimated as a difference between the effective solvation energy of the ligand in the complex with receptor as compared to the aqueous solution environment. The polar solvation energy is computed using the Poisson–Boltzmann surface area (PBSA) continuum electrostatics method. In this work, we did not consider the entropic component of the binding free energy. Moreover, the protein dielectric constant (chosen to be 8 here) is chosen empirically, which is known to vary depending on the local electrostatic environment in a protein. However, MM/PBSA method has proven to a computationally efficient and powerful method to reproduce the qualitative trends in the ligand binding affinity across multiple ligands, and also to dissect the relative contributions of the electrostatic, Van der Waals' and solvation terms to the binding energy.

Results and discussion

Effect of ebselen and diphenyl diselenide (DPDSe) on the activity of AChE

To investigate the mechanism of action of ebselen (control) and DPDSe (drug), kinetic assays of AChE were performed. Initial velocity of each progress curve observed was calculated in the first 30 seconds of the kinetic run. Lineweaver-Burk double reciprocal plots, using the initial velocities obtained over a range of substrate concentrations (10-100μM) were plotted for determination of various kinetic parameters in the absence and presence of the inhibitor compounds (DPDSe and Ebselen). Linear regression analysis was carried out for determination of kinetic parameters K_m, V_{max}, K_i and K_I from the Lineweaver-Burk and secondary plots. In case of both the inhibitors, double reciprocal primary plots (Fig. 2) showed intersection to the left of the $1/V_0$ axis and above the $1/S_0$ axis and thus exhibited mixed type of inhibition. K_I values, representing the inhibitor constant for enzyme inhibitor complex, were calculated from the linear regression analysis of $1/V_{max}$ vs. inhibitor concentration, whereas K_I was determined as the intercept on the X-axis (Fig. S1). Additionally, slope of primary plot against the inhibitor concentration was plotted to calculate K_i as an intercept on the I_0 axis (Fig. S1). Analysis of the obtained plots, revealed K_i values to be 21.30 and 43.28 and K_I of 65.01 and 193.92 in the presence of DPDSe and ebselen, respectively (Table 1). Both K_i and K_I values in the presence of DPDSe were found to be lower than that of the ebselen (Table 1). However, both DPDSe and ebselen decreased the activity of acetylcholinesterase by decreasing the V_{max} and increasing K_m (Fig. S2).

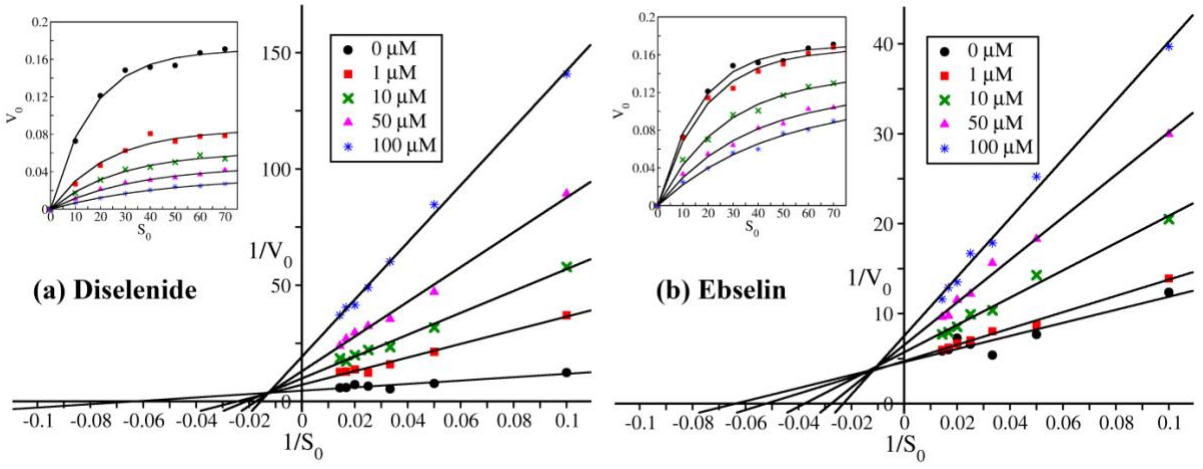

Figure 2. Lineweaver-Burk plots of AChE activity in presence of (a) Diselenide (DPDSe) and (b) Ebselen at various concentrations: 0 µM (black), 1 µM (red), 10 µM (green), 50 µM (magenta) and 100 µM (blue). Inset represents the Michaelis–Menten plots of AChE in presence of DPDSe and Ebselen.

Table 1. Enzyme kinetic parameters for mixed inhibition.

Name of Inhibitor	Concentration (µM)	K_m (µM)	V_{max}	K_I	K_I
DPDSe	0	21.18 ± 1.12	0.232 ± 0.02	21.30 ± 1.38	65.01 ± 4.95
	1	40.71 ± 2.81	0.139 ± 0.01		
	10	47.39 ± 4.75	0.101 ± 0.009		
	50	57.43 ± 3.36	0.077 ± 0.005		
	100	79.67 ± 6.23	0.060 ± 0.003		
Ebselen	1	19.18 ± 1.51	0.212 ± 0.02	43.28 ± 3.01	193.92 ± 15.51
	10	26.58 ± 2.02	0.175 ± 0.01		
	50	36.31 ± 2.94	0.153 ± 0.01		
	100	46.55 ± 4.09	0.140 ± 0.008		

However, as compared to ebselen, a sharp increase in K_m with a decrease in V_{max} was observed at lower concentrations of DPDSe. As can be seen in Fig. 2 and Table 1, a sharp decrease in enzyme activity at lower concentration of the inhibitor was observed wherein

the slope of the decrease is more in case of DPDSe. Results do infer enhanced DPDSe induced AChE inhibition in a concentration dependent manner with increasing K_m value from 21.18µM to 79.67µM and a decreasing V_{max} from 0.23 to 0.06. The lower value of inhibitor constants for DPDSe than that of ebselen infers stronger inhibition capability of DPDSe and thus proves it to be more potent inhibitor for AChE.

Effect of ebselen and DPDSe on the intrinsic fluorescence of AChE

Intrinsic fluorescence measurements were carried out to monitor change in overall tertiary structure of acetylcholinesterase in presence of the ebselen and DPDSe as inhibitor compounds (Fig. S3). Upon excitation at 280nm, the emission was recorded between 300nm to 500nm with a maximum at 334nm. In presence of increasing concentrations of DPDSe, enhanced fluorescence intensity was observed than that for control. As compared to control, a large increase in fluorescence intensity with a prominent wavelength shift was observed in presence of different concentrations of DPDSe. However, ebselen reduced the fluorescence intensity of AChE with a marked red shift of 8nm in the tryptophan emission. The observed decrease in the fluorescence intensity is most likely due to the quenching of tryptophan fluorescence by the exposed hydrophobic patches. The inhibitors binding to or near the tryptophan containing regions could be responsible for this observed changes in the fluorescence emission. We speculate that these structural changes could lead to decreased accessibility of substrate for the enzyme active site, or the DPDSe could affect the active site dynamics allosterically from a distal site. In order to gain further molecular insights into the observed structural and functional changes in acetylcholinesterase after its interaction with DPDSe as compared to the ebselen as control, we have carried out comprehensive *in silico* investigation using molecular docking and simulations.

Molecular docking analysis

Molecular docking studies of ebselen and DPDSe were performed to explore the possible interactions between the compounds and the active site of AChE. Two different poses for each ligand were obtained using the Schrodinger Glide program. The compounds were observed to bind near the catalytic active site (H444, S200 and E331) of AChE with

negative values of docking scores (Table S1). In order to compare the binding efficacy between ebselen and DPDSe, binding energy calculations were performed with the best predicted binding pose (Fig. S4). While rigid docking protocol is quite useful in identifying the putative binding poses, the accuracy of binding mode and energy strongly depends on the flexible neighbouring residues of the binding site. Hence, we have performed molecular dynamics (MD) simulations with the top-docking scored pose of ebselen and DPDSe at the active site of AChE to account for conformational flexibility of the neighbouring residues. The binding energy calculations were performed for the trajectory segments with the ligand position stable in the gorge using MM/PBSA method. Previous docking and simulation studies with known inhibitors and Ach reported binding energy between -5kcal/mol and -60kcal/mol[55-57]. We have observed the binding energy for ebselen and DPDSe from the MD snapshots as -32.17kcal/mol and -24.98kcal/mol respectively. It is evident from the results that electrostatics and van der Waals energy component have higher values for ebselen as compared to the DPDSe (Table S2). This is due to the presence of polar atoms and associated specific interactions (hydrogen bonds) of ebselen with the gorge residues. Fig. S5 exhibits the interactions between the ligands (ebselen and DPDSe) with the neighbouring gorge residues. Interestingly, the experimental results suggest mixed type inhibition for DPDSe and higher inhibition capability as compared to ebselen. Therefore, we explore the possibility of allosteric inhibition for DPDSe using molecular dynamics simulations.

Identification of possible binding sites through MD simulation

Four independent unbiased atomistic molecular dynamics simulations were performed to explore the binding sites for both Ebselen and DPDSe to elucidate their mechanism of inhibition for AChE. The pathways of the DPDSe molecule were tracked from the solution to the binding sites in AChE to identify/explore the possible sites of protein-ligand interactions. In all the simulations, DPDSe was placed at a random position in the solution at least 2nm away from the gorge entry in random orientation. The simulation setup contained no prior knowledge of the catalytic site and ACh binding pathway, which results in an unbiased exploration of the AChE protein by the ligand and its binding affinity at different interaction sites.

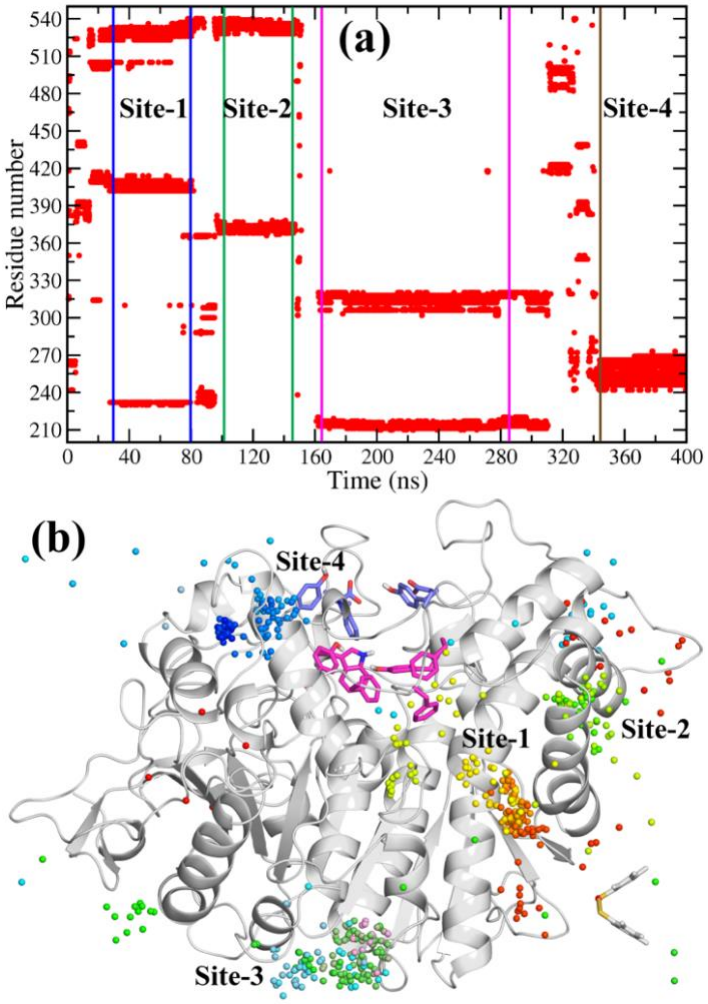

Figure 3. (a) Contact analysis between the diselenide and AChE protein for the trajectory mol-1a and existence of multiple interaction sites over the protein surface. (b) Visual representation of the four different sites identified in the mol-1a trajectory. The residues from PAS (peripheral anionic site) and neck are coloured in blue and magenta respectively, in the sticks representation. The position of a ligand at a particular time is shown as sphere. The time evolution of the position (sphere) from the beginning to the end of the simulation is depicted using colour gradient from red to green to blue. The spheres form clusters at four different sites representing the binding sites.

One of the principle strategies to inhibit the functional activity of enzymes is by blocking the active site using competitive inhibitors. Several inhibitors approved as drugs, and

promising candidates in clinical trials which have reached testing phase target AChE in a similar manner. To examine whether DPDSe binds the active site of AChE, distance between the ligand and the active site (binding pocket) as a function of time was monitored (Fig. S6). Interestingly, it was observed that in one (mol-1b, red) of the two trajectories, the DPDSe molecule after occasionally binding at the protein surface enters the active site of AChE. In another exploratory simulation (mol-1a, black), the ligand does not enter the cavity and forms contact with the protein surface for the entire trajectory with the minimum interatomic distance between ligand and protein less than 0.3nm (Fig. S7). For this trajectory (mol-1a), amino acid residues that are in contact with the DPDSe as a function of time were identified (Fig. 3a). As depicted in Fig. 3a, the ligand interacts with AChE at four distinct sites other than the active site of the AChE at different time intervals, i.e. site-1 (30ns-80ns), site-2 (100ns-140ns), site-3 (170-290ns) and site-4 (350-400ns). The site-1 and site-2 stand by the gorge on the helix-bundle, site-3 underpins the gorge, and site-4 is on the top of gorge (3-helix bundle) in the opposite direction of site-2. It is evident from Fig. S6 and 3b that these sites are distantly located from the catalytic triad or gorge. Evidences from structural and biochemical studies suggest ligand binding sites located at a distance from the catalytic centre can modulate the activity of AChE in an allosteric manner[58-60]. Several therapeutic inhibitors and allosteric activators bind to these sites and inhibit catalysis either by blocking the entry of substrate or by allosteric alteration of the conformation of the active site. Here, we investigate whether the identified putative ligand binding sites can play a role in allosteric regulation of AChE activity.

We must note here that for the trajectory depicted in Fig.3, the ligand explores the interaction sites intermittently without strongly attaching to any of them. However, other independent simulations (Fig. S12) demonstrate that indeed some of these sites can have significant residence time (>500ns). The variation across trajectories is due to the inherent stochastic nature of the ligand sampling, where the ligand may need to overcome an entropic bottleneck to find a specific cavity to open up. In Fig.4, we demonstrate the distance profile of the ligand from the PAS residues to show that both Ebselen and DPDSe can strongly bind to this site and participate in π-stacking and cation-π

interactions with the large number of aromatic side-chains that exist along the gorge as well as arginines in some cases.

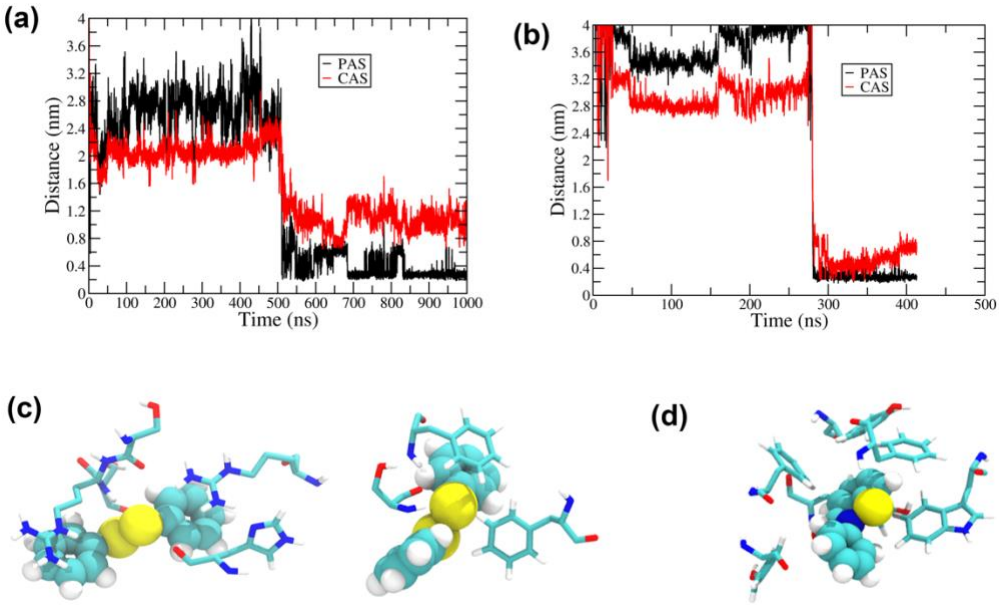

Figure 4. Minimum distance between the Se atoms of the ligand and the PAS residues (D71 and W283) for (a) Ebselen and (b) DPDS indicating that ligands eventually find the PAS binding site and remains tightly bound during the observation time. The representative binding poses with interacting amino acid residues are shown for (c) DPDSe and (d) Ebselen. Clearly, interactions with aromatic residues including tryptophan (W283 of PAS) and charged residue like arginine facilitate the binding.

Structural deviation and fluctuations between apo and ligand bound AChE

Earlier studies suggest that structural fluctuations play a significant role in the functional activity of AChE. As compared to apo form, binding of inhibitors at catalytic and peripheral site (ligand bound AChE) results in restrained or enhanced movements in different regions of AChE. The thermal fluctuations in the gorge in the *apo* form are described as breathing motions in the literature[61]. To analyze the dynamical and structural changes upon ligand binding at different sites in the trajectory mol-1a, we have performed clustering and principal component analysis (PCA) for the *apo* and bound form of AChE with DPDSe. The bound trajectory was dissected into different segments based on the

time intervals for which the ligand was bound to AChE. Comparing them with the results of the *apo* form would help us to identify correlated motions or dominant conformational changes in different regions of AChE upon ligand binding.

The DPDSe-bound AChE conformations were clustered individually from the trajectory segments and the middle structures with the least RMSD from the most populated clusters were superimposed for structural comparison and analysis. AChE exhibit structural deviations at four regions highlighted as L1-L4 in Fig. S8. Interestingly, L1 region corresponds to the omega loop which is known to exhibit enhanced fluctuations upon ligand interactions in AChE. Further, we observe that the binding site of DPDSe (Site-4) overlaps with the L4 loop region. In addition to the structural deviations, the associated fluctuations upon ligand binding were analyzed from PCA calculations. For this, fluctuations corresponding to the first five eigen vectors in the apo and bound state were analyzed. Fig. S9 compares the RMSF corresponding to first eigen vector between the *apo* form and the trajectory segments from different binding sites. It is evident from the results that the ligand binding at distinct sites on the protein surface enhances fluctuations in the residues that constitute part of the gorge and at distant sites from the gorge. We observe increase in the fluctuations of the residues (72-84) that belong to the omega loop which are also implicated in side door exit. Previous studies based on AChE inhibition by Fasciculin suggested enhanced fluctuations in the omega loop on ligand binding[17]. These large fluctuations of the omega loop affect the structural integrity of the main gorge as the residues of this loop make up one side of the gorge resulting in the inactivation of the AChE. In contrast, several allosteric inhibitors result in the rigidity of the omega loop modulating the side door closing/opening state. In addition to the omega loop, the residues that form the part of other loops of AChE with increased flexibility are shown as projections in Fig. 5.

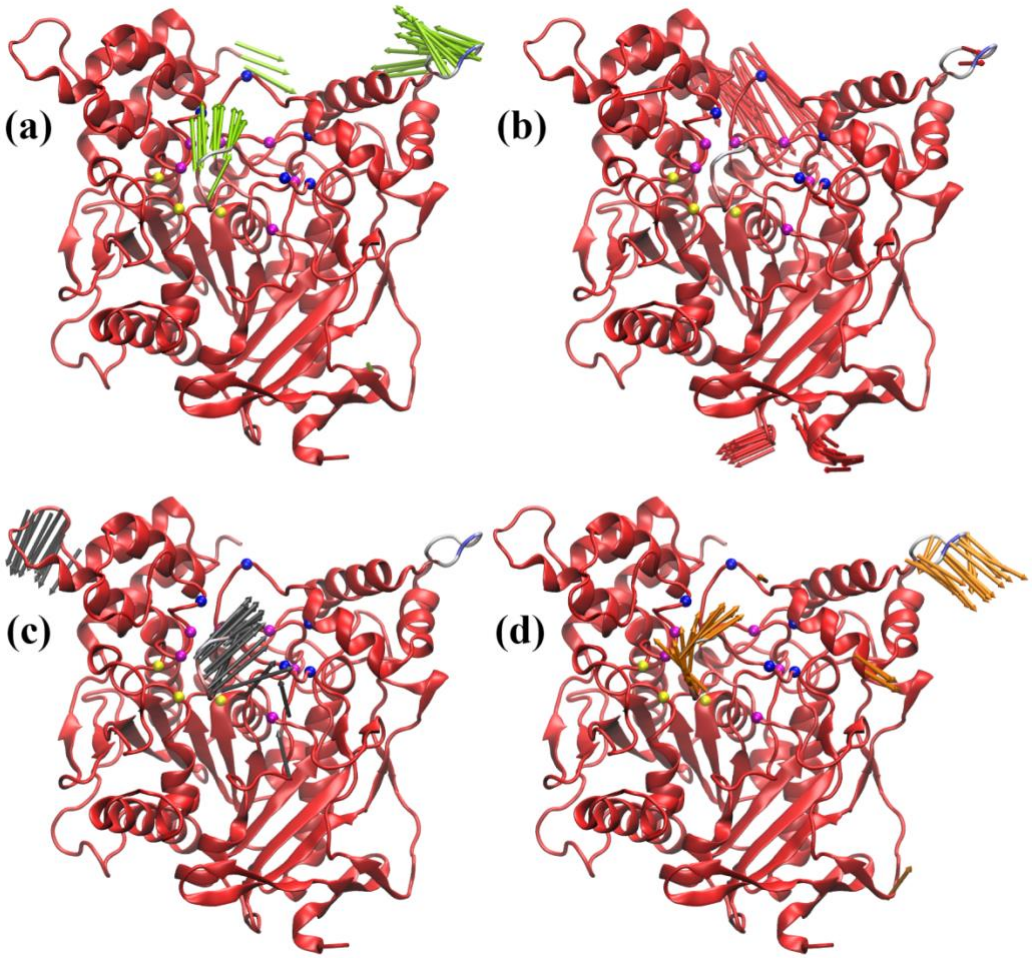

Figure 5. (a-d) Representation of structural variations along the dominant PCA-1 mode for all the four binding sites in mol-1a system. The projections represent regions with high degree of fluctuations. The important residues from the gorge and active site are represented as spheres in different colors: magenta (PAS residues), blue (neck residues) and yellow (catalytic residues). We observe large fluctuations in the omega loop (69-96) and residues 256-261 upon ligand binding.

Recently, a microsecond long simulation study identified sub-domains including omega loop whose dynamics are correlated with the gorge radius and subsequent breathing motions in AChE[21]. We were able to show the binding sites identified in our simulation mapped onto the AChE along with the sub-domains identified by Cheng and co-workers[21] (Fig. S10). It was observed that the binding sites for DPDSe in trajectory mol-1a are adjacent to the sub-domain residues that form the inner wall of the gorge. Interestingly,

the binding site-4 constitutes residues which are part of the S2 sub-domain. The binding site residues show enhanced rigidity due to ligand binding, however at the same time, increase flexibility of the loop residues that form the part of peripheral anionic site (Fig. S9d). Similarly, residues from site-1 and site-2 are adjacent to the S3 sub-domain and the catalytic triad. It is possible that the ligand binding at outer protein surface can modify the flexibility/rigidity of the protein in such a way that the conformation of the active site/gorge is modulated from its normal behaviour and thus allosterically control the activity of AChE.

Multiple possible pathways and binding sites for DPDSe entry into gorge

One of the key findings from our simulation is that the DPDSe molecule can enter the gorge cavity and occupy the active site in trajectory mol-1b. Fig. 6 illustrates the time evolution of the DPDSe molecule as it reaches the binding site. It was observed that ligand binds at the outer surface (site-5) of the protein during the initial phase of the simulation for a short time interval from 85-120ns. Interestingly, we observed that, unlike substrate/inhibitors which enter the cavity through the main gorge, the ligand (DPDSe) moves from the initial binding site to the interior of the gorge through the "side door" composed of residues from the Ω loop instead of the usual substrate entry point of the gorge. Further, it was observed that the DPDSe molecule remains trapped in the gorge during the rest of the simulation. Earlier studies highlight that in addition to the usual exit routes i.e., main gorge and back door, several small ligand molecules (ammonium ion, methane, thiocholine) were found to exit through the side door[19]. The movement of ligand molecule through the side door will involve torsional motions and fluctuations which will contribute to the transient conformational changes of the Ω loop[20]. Results obtained in our study do infer that inhibition of AChE by DPDSe involves a distinct pathway for the entry of the inhibitor to the active site.

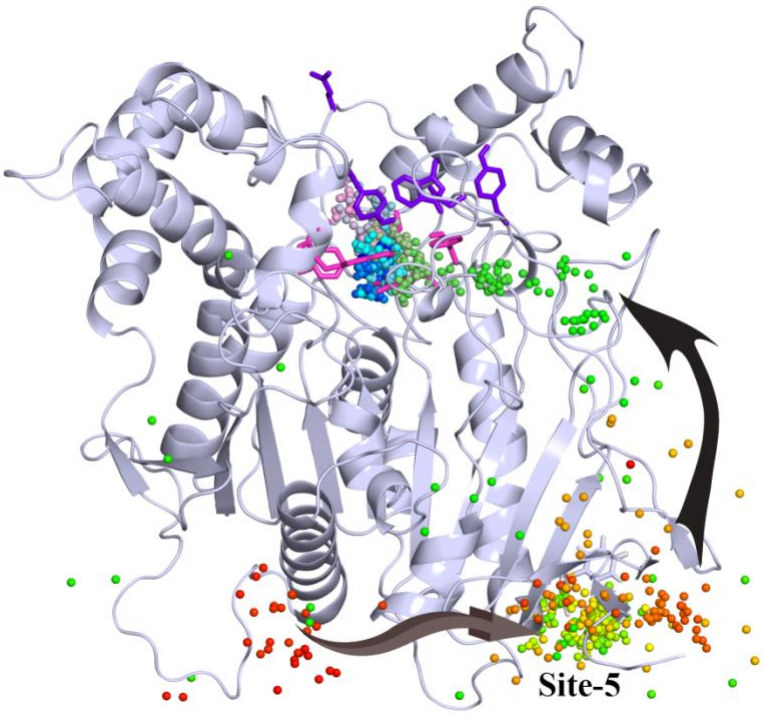

Figure 6. A representative trajectory for the ligand entry into the gorge through the side door. The figure shows the time evolution of the ligand in the system for the trajectory mol-1b. The position of a ligand at a particular time is shown as sphere. The time evolution of the position (sphere) from the beginning to the end of the simulation is depicted using color gradient from red to green to blue. Initially the ligand was present at site-5. However, eventually it detaches from this site to finally enter the interior of the gorge through the side door.

Previous studies highlight the role of gating residues (W83, Y121, F330, Y334) in the exit of the ligands (e.g. ammonium ions) through the back/side door and product release through the main gorge[19]. The gating residues Y121 and F334 forms a constriction/bottleneck that act as gate for the entry or exit of ligand molecules along the main gorge[9,11]. This is complemented by a rotational displacement of W83 that regulates the back door opening/closing. Here, we show that a similar mechanism involving gating residues (W83, Y121, Y334), that exhibit side chain motion necessary for side door opening and closing followed by trapping of DPDSe (ligand) inside the gorge. Fig. S11 shows the time evolution of chi angles that capture the orientation of the sidechain along

the simulation. Based on this figure, it is evident that entry of the ligand results in the change in the orientation of the W83, Y121 and Y334 residues. Fig. 7 exhibits the mechanism in an illustrative form where it was observed that the change in the orientation of W83 facilitates entry of the DPDSe ligand followed by the concerted change in the orientation of W83, Y121 and Y334 to trap the DPDSe ligand inside the gorge.

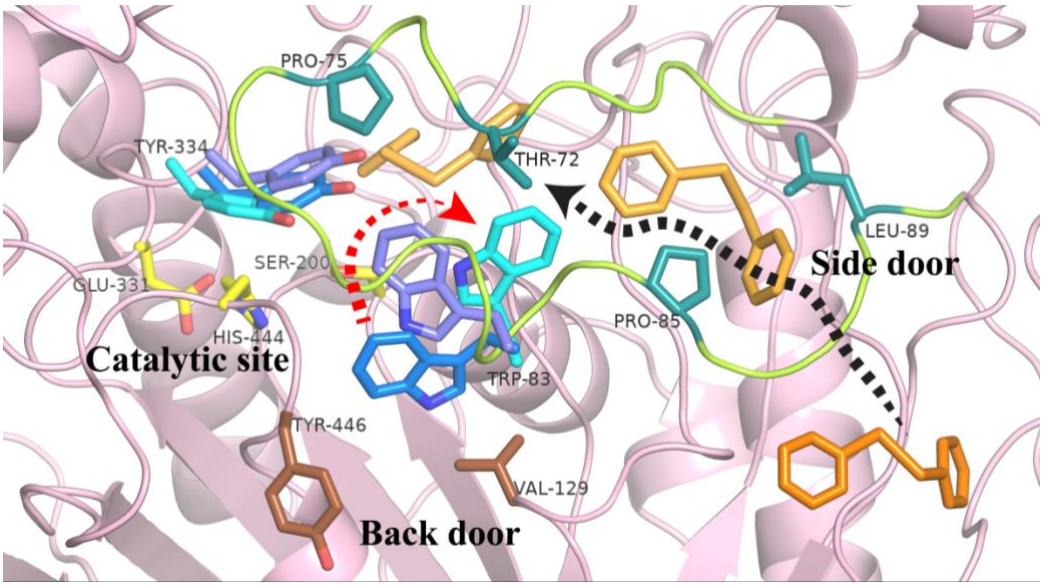

Figure 7. Gating mechanism for ligand entry through side door in an illustrative form. The omega loop is highlighted in green color. The entry of the ligand results in the change in the orientation of the W83 which is followed by the change in the orientation of Y334. Together these two residues capture the ligand inside the gorge.

However, we must clarify that the results depicted in Figs.6-7 present observations from a single representative trajectory. We do not have sufficient statistics to comment on a dominant pathway for the ligand entry. However, the multiple independent simulations as presented in Fig. S12 show that all of the interaction sites identified and presented here have significant population in the overall cumulative trajectory set. In particular, the strong binding to PAS region for both DPDSe and Ebselen is a statistically significant result that explains the non-competitive mode of inhibition for these organoselenium compounds.

Binding energies for different ligand interaction sites

The binding energy for the DPDSe ligand and its interaction at different sites in both the trajectories (mol-1a and mol-1b) was calculated by MM-PBSA method from MD snapshots. The mol-1a trajectory segments include site-1 (40-65ns), site-2 (98-108ns), site-3 (277-286ns) and site-4 (350-365ns). The ligand binding sites in mol-1b trajectory are site-5 (85-115ns) and DPDSe inside the cavity/gorge (235-855ns). The binding energy for the DPDSe molecule is shown in Table 2. It seems quite evident from binding energy calculations that as compared to the electrostatic component, the van der Waals energy significantly contributes to the inhibition of AChE by DPDSe. It was observed that the binding energy of DPDSe over the protein surface at site-1 (-14.6 kcal/mol), site-2 (-12.29 kcal/mol) and site-5 (-14.0 kcal/mol) is comparatively lower than that at site-3 (-20.78 kcal/mol) and site-4 (-23.31 kcal/mol). Interestingly the binding energy of diselenide (-25.8 kcal/mol) inside the gorge is quite comparable to that of the known calculated value for ACh (-27.18 kcal/mol) from earlier study based on 100ps FEP simulation[55]. However, these results come with a caveat that MM/PBSA estimate of binding energy does not include the entropic effect which is often plays an important role in overall binding free energy. But these estimates provide a qualitative comparison between these two ligands and also the relative contribution of various types of interactions namely electrostatic, Van der Waals', polar/non-polar solvation etc. Clearly, as observed earlier through the binding modes, both ligands prefer to interact with the aromatic residues and arginine. Thus, the π-stacking and cation-π interactions seem to play an important role in the binding affinity of these inhibitors.

Table 2. Binding energy calculation for the ligand (diselenide) using MM/PBSA approach. In a previous study, the binding free energy for ACh was found to be -27.2 kcal/mol based on 100ps FEP simulation[55]. The error bars are computed from the standard deviation of the respective energy terms over the trajectory.

System	**Mol-1a** (All binding sites outside cavity)				**Mol-1b**	
Summary (kcal/mol)	**Site-1**	**Site-2**	**Site-3**	**Site-4**	**Site-5**	Inside-gorge
van der Waal energy	-18.7 +/- 0.30	-19.4 +/- 0.20	-26.4 +/- 0.18	-31.7 +/- 0.24	-17.9 +/- 0.11	-30.2 +/- 0.05
Electrostatic energy	-3.3 +/- 0.24	-3.9 +/- 0.19	-8.4 +/- 0.19	-4.1 +/- 0.14	-5.5 +/- 0.20	-7.3 +/- 0.05
Polar solvation energy	9.7 +/- 0.40	13.3 +/- 0.19	16.7 +/- 0.14	15.3 +/- 0.14	11.4 +/- 0.14	14.6 +/- 0.04
SASA energy	-2.4 +/- 0.03	-2.4 +/- 0.01	-2.7 +/- 0.02	-2.9 +/- 0.02	-2.0 +/- 0.01	-2.9 +/- 0.00
Binding energy (kcal/mol)	**-14.6 +/- 0.33**	**-12.3 +/- 0.25**	**-20.8 +/- 0.20**	**-23.3 +/- 0.29**	**-14.0 +/- 0.15**	**-25.8 +/- 0.07**

Conclusions

The present study provides a detailed molecular perspective into the inhibition mechanism for AChE by organoselenium compounds (ebselen and DPDSe). We have comprehensively investigated the binding mechanism and mode of action of both the inhibitors to AChE using multiple approaches including enzyme kinetics, intrinsic fluorescence, molecular docking and simulation studies. The results obtained by the kinetic studies revealed that both the inhibitors exhibit mixed type of inhibition where DPDSe has stronger inhibition capability as compared to the ebselen compound. Intrinsic fluorescence measurements suggest reduced enzyme activity attributed to the enhanced conformational flexibility and altered structural conformations upon the binding of ebselen and DPDSe due to binding to sites rich in aromatic residues including tryptophan. Here, we present molecular insights into the enzyme-inhibitor interactions and predict energetically stable ligand binding modes based on in silico methods of molecular docking and simulation.

We have performed cumulative several microseconds long simulations of the enzyme-inhibitor system with Ebselen and DPDSe to explore the additional binding sites as a means of allosteric regulation of AChE activity. To our surprise, the DPDSe molecule interacts with 4-5 distinct sites over AChE protein surface with varying degree of binding energy and elucidates the change in conformational fluctuations of the inhibitor-bound complex. It is apparent from structural deviations and fluctuation analysis that the motions of the omega loop and other remote regions could allosterically exert significant influence on the gorge fluctuations and structural integrity of the gorge. Interestingly, we observed an unusual entry point of the inhibitor (DPDSe) into the gorge through the side door involving a ligand gated mechanism. It is concluded that the gating residues (W83, Y121, F330, Y334) move in concert with each other to play an important/predominant role in the entry of DPDSe molecule into the active-site gorge. Using MM/PBSA method we obtain an approximate estimate of the binding energy at -32.2 kcal/mol (ebselen) and -25.0 kcal/mol (DPDSe) for ligands docked at the catalytic active site inside gorge. The binding energies were also determined for the multiple interaction sites for the DPDSe-AChE complex.

Most importantly, we elucidate that the non-competitive mode of inhibition occurs due to the strong propensity of these organoselenium compounds to bind to the PAS region of AChE (near the mouth of the gorge). A combination of π-stacking and cation-π interactions with aromatic residues lining the gorge and arginines is responsible for the ligand binding. This is consistent with the known PAS binding inhibitors that also exhibit a mixed inhibition mechanism. Thus, our observations from MD simulations reveal mixed type of inhibition for DPDSe on the activity of AChE, which are consistent with our experimental results and contribute to the better understanding of the therapeutic potential of DPDSe compound. In addition, our simulation trajectories reveal several distal interaction sites suitable as drug targets. Although the dissociation kinetics of inhibitors was fast for some of these sites, but our observations would be useful in future design of more optimised allosteric inhibitors using these sites as possible drug targets.

Conflicts of interest

There are no conflicts to declare.

Supporting Information

Additional experimental and computational data including Secondary Lineweaver Burk plots, intrinsic fluorescence data, docking poses and interactions, analysis of independent ligand trajectories and protein dynamics

Acknowledgements

SC thanks SERB, DST, India for funding (project code: ECR/2018/002903). AK thanks SNBNCBS for postdoctoral fellowship. Authors thank SNBNCBS, Kolkata for the supercomputing facility.

References

(1) Silman, I.; Sussman, J. L. Acetylcholinesterase:'classical'and 'non-classical'functions and pharmacology. *Current opinion in pharmacology* **2005,** *5* (3), 293.

(2) Colletier, J. P.; Fournier, D.; Greenblatt, H. M.; Stojan, J.; Sussman, J. L.; Zaccai, G.; Silman, I.; Weik, M. Structural insights into substrate traffic and inhibition in acetylcholinesterase. *The EMBO journal* **2006,** *25* (12), 2746.

(3) Millard, C. B.; Broomfield, C. A. Anticholinesterases: medical applications of neurochemical principles. *Journal of neurochemistry* **1995,** *64* (5), 1909.

(4) Rotundo, R. L. Expression and localization of acetylcholinesterase at the neuromuscular junction. *Journal of neurocytology* **2003,** *32* (5-8), 743.

(5) Kryger, G.; Silman, I.; Sussman, J. L. Structure of acetylcholinesterase complexed with E2020 (Aricept®): implications for the design of new anti-Alzheimer drugs. *Structure* **1999,** *7* (3), 297.

(6) Bajda, M.; Więckowska, A.; Hebda, M.; Guzior, N.; Sotriffer, C. A.; Malawska, B. Structure-based search for new inhibitors of cholinesterases. *International journal of molecular sciences* **2013,** *14* (3), 5608.

(7) Anand, P.; Singh, B. A review on cholinesterase inhibitors for Alzheimer's disease. *Archives of pharmacal research* **2013,** *36* (4), 375.

(8) Wlodek, S. T.; Clark, T. W.; Scott, L. R.; McCammon, J. A. Molecular dynamics of acetylcholinesterase dimer complexed with tacrine. *Journal of the American Chemical Society* **1997,** *119* (40), 9513.

(9) Niu, C.; Xu, Y.; Xu, Y.; Luo, X.; Duan, W.; Silman, I.; Sussman, J. L.; Zhu, W.; Chen, K.; Shen, J. Dynamic mechanism of E2020 binding to acetylcholinesterase: a steered molecular dynamics simulation. *The Journal of Physical Chemistry B* **2005,** *109* (49), 23730.

(10) Antosiewicz, J.; Wlodek, S. T.; McCammon, J. A. Acetylcholinesterase: role of the enzyme's charge distribution in steering charged ligands toward the active site. *Biopolymers* **1996,** *39* (1), 85.

(11) Xu, Y.; Shen, J.; Luo, X.; Silman, I.; Sussman, J. L.; Chen, K.; Jiang, H. How does huperzine A enter and leave the binding gorge of acetylcholinesterase? Steered molecular dynamics simulations. *Journal of the American Chemical Society* **2003,** *125* (37), 11340.

(12) Tara, S.; Elcock, A. H.; Kirchhoff, P. D.; Briggs, J. M.; Radic, Z.; Taylor, P.; McCammon, J. A. Rapid binding of a cationic active site inhibitor to wild type and mutant mouse acetylcholinesterase: Brownian dynamics simulation including diffusion in the active site gorge. *Biopolymers: Original Research on Biomolecules* **1998,** *46* (7), 465.

(13) Wiesner, J.; Kříž, Z.; Kuča, K.; Jun, D.; Koča, J. Acetylcholinesterases–the structural similarities and differences. *Journal of enzyme inhibition and medicinal chemistry* **2007,** *22* (4), 417.

(14) Tõugu, V.; Kesvatera, T. Role of ionic interactions in cholinesterase catalysis. *Biochimica et Biophysica Acta (BBA)-Protein Structure and Molecular Enzymology* **1996,** *1298* (1), 12.

(15) Fang, L.; Pan, Y.; Muzyka, J. L.; Zhan, C.-G. Active site gating and substrate specificity of butyrylcholinesterase and acetylcholinesterase: insights from molecular dynamics simulations. *The Journal of Physical Chemistry B* **2011,** *115* (27), 8797.

(16) Gilson, M.; Straatsma, T.; McCammon, J.; Ripoll, D.; Faerman, C.; Axelsen, P.; Silman, I.; Sussman, J. Open" back door" in a molecular dynamics simulation of acetylcholinesterase. *Science* **1994,** *263* (5151), 1276.

(17) Bui, J. M.; Tai, K.; McCammon, J. A. Acetylcholinesterase: enhanced fluctuations and alternative routes to the active site in the complex with fasciculin-2. *Journal of the American Chemical Society* **2004,** *126* (23), 7198.

(18) Bourne, Y.; Grassi, J.; Bougis, P. E.; Marchot, P. Conformational flexibility of the acetylcholinesterase tetramer suggested by x-ray crystallography. *Journal of Biological Chemistry* **1999,** *274* (43), 30370.

(19) Van Belle, D.; De Maria, L.; Iurcu, G.; Wodak, S. J. Pathways of ligand clearance in acetylcholinesterase by multiple copy sampling. *Journal of molecular biology* **2000,** *298* (4), 705.

(20) Xu, Y.; Colletier, J.-P.; Weik, M.; Qin, G.; Jiang, H.; Silman, I.; Sussman, J. L. Long route or shortcut? A molecular dynamics study of traffic of thiocholine within the active-site gorge of acetylcholinesterase. *Biophysical journal* **2010,** *99* (12), 4003.

(21) Cheng, S.; Song, W.; Yuan, X.; Xu, Y. Gorge motions of acetylcholinesterase revealed by microsecond molecular dynamics simulations. *Scientific reports* **2017,** *7* (1), 1.

(22) Colovic, M. B.; Krstic, D. Z.; Lazarevic-Pasti, T. D.; Bondzic, A. M.; Vasic, V. M. Acetylcholinesterase inhibitors: pharmacology and toxicology. *Current neuropharmacology* **2013,** *11* (3), 315.

(23) Mathew, B.; Parambi, D. G.; Mathew, G. E.; Uddin, M. S.; Inasu, S. T.; Kim, H.; Marathakam, A.; Unnikrishnan, M. K.; Carradori, S. Emerging therapeutic potentials of dual-acting MAO and AChE inhibitors in Alzheimer's and Parkinson's diseases. *Archiv der Pharmazie* **2019,** *352* (11), 1900177.

(24) Akhoon, S. A.; Naqvi, T.; Nisar, S.; Rizvi, M. A. Synthetic Organo-Selenium Compounds in Medicinal Domain. *Asian Journal of Chemistry* **2015,** *27* (8).

(25) Rizvi, M. A.; Guru, S.; Naqvi, T.; Kumar, M.; Kumbhar, N.; Akhoon, S.; Banday, S.; Singh, S. K.; Bhushan, S.; Peerzada, G. M. An investigation of in vitro cytotoxicity and apoptotic potential of aromatic diselenides. *Bioorganic & medicinal chemistry letters* **2014,** *24* (15), 3440.

(26) Rizvi, M. A.; Zaki, M.; Afzal, M.; Mane, M.; Kumar, M.; Shah, B. A.; Srivastav, S.; Srikrishna, S.; Peerzada, G. M.; Tabassum, S. Nuclear blebbing of biologically active organoselenium compound towards human cervical cancer cell (HeLa): In vitro

DNA/HSA binding, cleavage and cell imaging studies. *European journal of medicinal chemistry* **2015,** *90*, 876.

(27) Nogueira, C. W.; Zeni, G.; Rocha, J. B. Organoselenium and organotellurium compounds: toxicology and pharmacology. *Chemical Reviews* **2004,** *104* (12), 6255.

(28) Martini, F.; Augusto Bruning, C.; Mendonca Soares, S.; Wayne Nogueira, C.; Zeni, G. Inhibitory effect of ebselen on cerebral acetylcholinesterase activity in vitro: kinetics and reversibility of inhibition. *Current pharmaceutical design* **2015,** *21* (7), 920.

(29) Martini, F.; Pesarico, A. P.; Brüning, C. A.; Zeni, G.; Nogueira, C. W. Ebselen inhibits the activity of acetylcholinesterase globular isoform G4 in vitro and attenuates scopolamine-induced amnesia in mice. *Journal of cellular biochemistry* **2018,** *119* (7), 5598.

(30) Pinton, S.; da Rocha, J. T.; Zeni, G.; Nogueira, C. W. Organoselenium improves memory decline in mice: involvement of acetylcholinesterase activity. *Neuroscience letters* **2010,** *472* (1), 56.

(31) Luo, Z.; Sheng, J.; Sun, Y.; Lu, C.; Yan, J.; Liu, A.; Luo, H.-b.; Huang, L.; Li, X. Synthesis and evaluation of multi-target-directed ligands against Alzheimer's disease based on the fusion of donepezil and ebselen. *Journal of medicinal chemistry* **2013,** *56* (22), 9089.

(32) Girek, M.; Szymański, P. Tacrine hybrids as multi-target-directed ligands in Alzheimer's disease: influence of chemical structures on biological activities. *Chemical Papers* **2019,** *73* (2), 269.

(33) Wang, Z.; Li, W.; Wang, Y.; Li, X.; Huang, L.; Li, X. Design, synthesis and evaluation of clioquinol–ebselen hybrids as multi-target-directed ligands against Alzheimer's disease. *RSC advances* **2016,** *6* (9), 7139.

(34) Rosa, R. M.; Roesler, R.; Braga, A. L.; Saffi, J.; Henriques, J. A. P. Pharmacology and toxicology of diphenyl diselenide in several biological models. *Brazilian Journal of Medical and Biological Research* **2007,** *40* (10), 1287.

(35) Posser, T.; Franco, J. L.; dos Santos, D. A.; Rigon, A. P.; Farina, M.; Dafré, A. L.; Rocha, J. B. T.; Leal, R. B. Diphenyl diselenide confers neuroprotection against hydrogen peroxide toxicity in hippocampal slices. *Brain research* **2008,** *1199*, 138.

(36) Pinton, S.; da Rocha, J. T.; Gai, B. M.; Prigol, M.; da Rosa, L. V.; Nogueira, C. W. Neuroprotector effect of p, p'-methoxyl-diphenyl diselenide in a model of sporadic dementia of Alzheimer's type in mice: contribution of antioxidant mechanism. *Cell biochemistry and function* **2011,** *29* (3), 235.

(37) Pinton, S.; Brüning, C. A.; Oliveira, C. E. S.; Prigol, M.; Nogueira, C. W. Therapeutic effect of organoselenium dietary supplementation in a sporadic dementia of Alzheimer's type model in rats. *The Journal of nutritional biochemistry* **2013,** *24* (1), 311.

(38) Pandey, A.; Rizvi, M.; Shah, B. A.; Bani, S. Anti-arthritogenic effect of Saponin-1 by alteration of Th1/Th2 cytokine paradigm in arthritic mice. *Cytokine* **2016,** *79*, 103.

(39) Rizvi, M. A.; Hussain, Z.; Ali, F.; Amin, A.; Mir, S. H.; Rydzek, G.; Jagtap, R. M.; Pardeshi, S. K.; Qadri, R. A.; Ariga, K. Bioactive Supra Decorated Thiazolidine-4-carboxylic acid derivative attenuates cellular oxidative stress by enhancing catalase activity. *Physical Chemistry Chemical Physics* **2020**, DOI:10.1039/D0CP00253D 10.1039/D0CP00253D.

(40) Ellman, G. L.; Courtney, K. D.; Andres Jr, V.; Featherstone, R. M. A new and rapid colorimetric determination of acetylcholinesterase activity. *Biochemical pharmacology* **1961,** *7* (2), 88.

(41) Friesner, R. A.; Murphy, R. B.; Repasky, M. P.; Frye, L. L.; Greenwood, J. R.; Halgren, T. A.; Sanschagrin, P. C.; Mainz, D. T. Extra precision glide: Docking and scoring incorporating a model of hydrophobic enclosure for protein− ligand complexes. *Journal of medicinal chemistry* **2006,** *49* (21), 6177.

(42) Abraham, M. J.; Murtola, T.; Schulz, R.; Páll, S.; Smith, J. C.; Hess, B.; Lindahl, E. GROMACS: High performance molecular simulations through multi-level parallelism from laptops to supercomputers. *SoftwareX* **2015,** *1-2*, 19.

(43) Lindorff-Larsen, K.; Piana, S.; Palmo, K.; Maragakis, P.; Klepeis, J. L.; Dror, R. O.; Shaw, D. E. Improved side-chain torsion potentials for the Amber ff99SB protein force field. *Proteins* **2010,** *78* (8), 1950.

(44) Horn, H. W.; Swope, W. C.; Pitera, J. W.; Madura, J. D.; Dick, T. J.; Hura, G. L.; Head-Gordon, T. Development of an improved four-site water model for biomolecular simulations: TIP4P-Ew. *The Journal of Chemical Physics* **2004,** *120* (20), 9665.

(45) Schmid, N.; Eichenberger, A. P.; Choutko, A.; Riniker, S.; Winger, M.; Mark, A. E.; van Gunsteren, W. F. Definition and testing of the GROMOS force-field versions 54A7 and 54B7. *European biophysics journal* **2011,** *40* (7), 843.

(46) Berendsen, H.; Postma, J.; Van Gunsteren, W.; Hermans, a. J.; Reidel, Dordrecht Jerusalem, Israel, 1981.

(47) Wang, J.; Wolf, R. M.; Caldwell, J. W.; Kollman, P. A.; Case, D. A. Development and testing of a general amber force field. *Journal of computational chemistry* **2004,** *25* (9), 1157.

(48) Malde, A. K.; Zuo, L.; Breeze, M.; Stroet, M.; Poger, D.; Nair, P. C.; Oostenbrink, C.; Mark, A. E. An automated force field topology builder (ATB) and repository: version 1.0. *Journal of chemical theory and computation* **2011,** *7* (12), 4026.

(49) Bussi, G.; Donadio, D.; Parrinello, M. Canonical sampling through velocity rescaling. *The Journal of Chemical Physics* **2007,** *126* (1), 014101.

(50) Parrinello, M.; Rahman, A. Polymorphic transitions in single crystals: A new molecular dynamics method. *Journal of Applied Physics* **1981,** *52* (12), 7182.

(51) Essmann, U.; Perera, L.; Berkowitz, M. L.; Darden, T.; Lee, H.; Pedersen, L. G. A smooth particle mesh Ewald method. *The Journal of Chemical Physics* **1995,** *103* (19), 8577.

(52) Hess, B.; Bekker, H.; Berendsen, H. J. C.; Fraaije, J. G. E. M. LINCS: A linear constraint solver for molecular simulations. *Journal of Computational Chemistry* **1997,** *18* (12), 1463.

(53) Baker, N. A.; Sept, D.; Joseph, S.; Holst, M. J.; McCammon, J. A. Electrostatics of nanosystems: application to microtubules and the ribosome. *Proceedings of the National Academy of Sciences* **2001,** *98* (18), 10037.

(54) Kumari, R.; Kumar, R.; Consortium, O. S. D. D.; Lynn, A. g_mmpbsa□ A GROMACS tool for high-throughput MM-PBSA calculations. *Journal of chemical information and modeling* **2014,** *54* (7), 1951.

(55) Nascimento, E. r. C.; Oliva, M. n.; Świderek, K.; Martins, J. o. B.; Andrés, J. Binding analysis of some classical acetylcholinesterase inhibitors: insights for a rational design using free energy perturbation method calculations with QM/MM MD simulations. *Journal of chemical information and modeling* **2017,** *57* (4), 958.

(56) Cavdar, H.; Senturk, M.; Guney, M.; Durdagi, S.; Kayik, G.; Supuran, C. T.; Ekinci, D. Inhibition of acetylcholinesterase and butyrylcholinesterase with uracil derivatives: kinetic and computational studies. *Journal of enzyme inhibition and medicinal chemistry* **2019,** *34* (1), 429.

(57) Kiametis, A. S.; Silva, M. A.; Romeiro, L. A.; Martins, J. B.; Gargano, R. Potential acetylcholinesterase inhibitors: molecular docking, molecular dynamics, and in silico prediction. *Journal of molecular modeling* **2017,** *23* (2), 67.

(58) Chierrito, T. P. C.; Pedersoli-Mantoani, S.; Roca, C.; Requena, C.; Sebastian-Perez, V.; Castillo, W. O.; Moreira, N. C. S.; Pérez, C.; Sakamoto-Hojo, E. T.; Takahashi, C. S.et al. From dual binding site acetylcholinesterase inhibitors to allosteric modulators: A new avenue for disease-modifying drugs in Alzheimer's disease. *European Journal of Medicinal Chemistry* **2017,** *139*, 773.

(59) Roca, C.; Requena, C.; Sebastián-Pérez, V.; Malhotra, S.; Radoux, C.; Pérez, C.; Martinez, A.; Antonio Páez, J.; Blundell, T. L.; Campillo, N. E. Identification of new allosteric sites and modulators of AChE through computational and experimental tools. *Journal of enzyme inhibition and medicinal chemistry* **2018,** *33* (1), 1034.

(60) Marcelo, F.; Dias, C.; Martins, A.; Madeira, P. J.; Jorge, T.; Florêncio, M. H.; Cañada, F. J.; Cabrita, E. J.; Jiménez-Barbero, J.; Rauter, A. P. Molecular Recognition of Rosmarinic Acid from Salvia sclareoides Extracts by Acetylcholinesterase: A New Binding Site Detected by NMR Spectroscopy. *Chemistry – A European Journal* **2013,** *19* (21), 6641.

(61) Zhou, H.-X.; Wlodek, S. T.; McCammon, J. A. Conformation gating as a mechanism for enzyme specificity. *Proceedings of the National Academy of Sciences* **1998,** *95* (16), 9280.

TOC Graphic